

# Chemical abundances and winds of massive stars in M31: a B-type supergiant and a WC star in OB 10

S.J. Smartt,<sup>1</sup> P.A. Crowther,<sup>2</sup> P.L. Dufton,<sup>3</sup> <sup>3</sup>☆ D.J. Lennon<sup>4</sup>, R.P. Kudritzki<sup>5,8</sup>, A. Herrero<sup>6,9</sup>, J.K. McCarthy<sup>7</sup>, F. Bresolin<sup>5</sup>.

<sup>1</sup>*Institute of Astronomy, University of Cambridge, Madingley Road, Cambridge CB3 0HA*

<sup>2</sup>*Department of Physics and Astronomy, University College London, Gower Street, London WC1E 6BT*

<sup>3</sup>*The Department of Pure and Applied Physics, The Queen's University of Belfast, Belfast BT7 1NN*

<sup>4</sup>*The Isaac Newton Group of Telescopes, Apartado de Correos 368, E-38700, Santa Cruz de La Palma, Canary Islands, Spain*

<sup>5</sup>*Institut für Astronomie und Astrophysik der Universität München, Scheinerstr.1, D-81679, München, Germany*

<sup>6</sup>*Instituto de Astrofísica de Canarias, E-38200, La Laguna, Spain*

<sup>7</sup>*Pixel Vision Inc., Advanced Imaging Sensors Division 4952 Warner Avenue, Suite 300, Huntington Beach, CA 92649*

<sup>8</sup>*Institute for Astronomy, University of Hawaii at Manoa, 2680 Woodlawn Drive, Honolulu, Hawaii 96822*

<sup>9</sup>*Departamento de Astrofísica, Universidad de La Laguna, E-38071 La Laguna, Tenerife, Spain*

Accepted Received ; in original form

## ABSTRACT

We present high quality spectroscopic data for two massive stars in the OB 10 association of M31, OB 10–64 (B0Ia) and OB 10-WR1 (WC6). Medium resolution spectra of both stars were obtained using the ISIS spectrograph on the William Herschel Telescope. This is supplemented with HST-STIS UV spectroscopy and Keck I HIRES data for OB 10–64. A non-LTE model atmosphere and abundance analysis for OB 10–64 is presented indicating that this star has similar photospheric CNO, Mg and Si abundances as solar neighbourhood massive stars. A wind analysis of this early B-type supergiant reveals a mass-loss rate of  $\dot{M} = 1.6 \times 10^{-6} M_{\odot} \text{yr}^{-1}$ , and  $v_{\infty} = 1650 \text{ km s}^{-1}$ . The corresponding wind momentum is in good agreement with the wind momentum – luminosity relationship found for Galactic early B supergiants.

Observations of OB 10-WR1 are analysed using a non-LTE, line-blanketed code, to reveal approximate stellar parameters of  $\log L/L_{\odot} \sim 5.7$ ,  $T_* \sim 75 \text{ kK}$ ,  $v_{\infty} \sim 3000 \text{ km s}^{-1}$ ,  $\dot{M}/(M_{\odot} \text{yr}^{-1}) \sim 10^{-4.3}$  adopting a clumped wind with a filling factor of 10%. Quantitative comparisons are made with the Galactic WC6 star HD 92809 (WR23) revealing that OB 10-WR1 is 0.4 dex more luminous, though it has a much lower C/He ratio ( $\sim 0.1$  versus 0.3 for HD 92809). Our study represents the first detailed, chemical model atmosphere analysis for either a B-type supergiant or a WR star in Andromeda, and shows the potential of how such studies can provide new information on the chemical evolution of galaxies and the evolution of massive stars in the local Universe.

**Key words:** stars:abundances – stars: early-type – stars: Wolf-Rayet – galaxies: M31 – stars:winds

## 1 INTRODUCTION

The observation and analysis of hot, luminous stars in the Milky Way and other Local Group galaxies allows the investigation of stellar evolution and mass-loss within different environments. For example, Wolf-Rayet (WR) stars, the chemically evolved descendants of massive OB stars, provide

keys to our understanding of massive stellar evolution and nucleosynthetic processes, e.g. Dessart et al. (2000).

Studies of the physical nature of the A and B-type supergiants can also place constraints on evolution models in the upper main-sequence regions, e.g. Venn (1995), McErlean, Lennon & Dufton (1999). A further use of the A and B-type supergiants is in using photospheric analysis to constrain the chemical composition of the interstellar medium in their host galaxies. They are visually the brightest quasi-stable objects in galaxies, and being descendants of massive OB-type main-sequence objects have small lifetimes (5–

☆ On leave of absence at the Isaac Newton Group of Telescopes, Apartado de Correos 368, E-38700, Santa Cruz de La Palma

20 Myr). Many elements visible in their photospheres should not be affected by internal mixing and contamination with core processed material (e.g. O (only slightly affected in AB-types), Mg, Si, S, Al, Ca, Fe, Ti, Cr, Ni; Venn et al. 2000, Smartt, Dufton & Lennon 1997). Further they can also provide new information on the distances of galaxies through the detailed study of the strengths of their radiatively driven winds using the wind momentum – luminosity relationship (WLR, e.g. Kudritzki et al. 1999). An investigation of the stellar wind properties of O-, B- and A-supergiants in Local Group galaxies with well defined distances will, therefore, allow us to test the concept of the WLR and its applicability for distance determinations.

Numerous surveys have identified OB and WR stars beyond the Magellanic Clouds, e.g. Massey et al. (1986); Moffat & Shara (1987), although little quantitative analysis has been carried out to date. The only detailed studies of Wolf-Rayet stars beyond the Magellanic Clouds have been studies of late WN stars in M33 by Smith et al. (1997) and Crowther et al. (1997). Bianchi et al. (1994) have published UV spectroscopy of OB-type supergiants in M31 and M33, while Monteverde et al. (1997; 2000) derived the oxygen abundance gradient in M33 from studies of B-type supergiants. An indication of the capabilities of 8m class telescopes has been presented by Muschielok et al. (1999) for three B-type supergiants in NGC 6822 using VLT. Recently, Venn et al. (2000) have analysed four A-type supergiants in M31, the first detailed stellar analysis in this galaxy.

The present work demonstrates the capabilities of 4m class telescopes by analysing the spectra of two massive stars in the OB 10 association of our nearest giant spiral, Andromeda (= M31 = NGC 224). OB 10 (van den Bergh 1964, Massey et al. 1986) is located at  $23.6'$  from the centre of M31, and has an apparent size of  $2 \times 1.0'$ . Assuming a distance to M31 of 783 kpc (Holland 1998, Stanek & Garnavich 1998, assumed throughout this paper) the association's projected size is hence  $\sim 450 \times 225$  pc. Its stellar content was investigated by Massey et al. (1986) (and later Massey et al. 1995), who found two Wolf-Rayet candidates, OB 10-WR1 (classified as WC6-7) and OB 10-WR2 (classified only as WN) and a late O-type supergiant (OB 10-150; O8.5Ia(f)). The presence of such massive stars implies that it is a very young association, having formed in the last  $\sim 5$  Myrs. The de-projected position of OB 10 would suggest it has a galactocentric distance of 5.9 kpc. Blair, Kirshner & Chevalier (1982) have determined an abundance gradient in M31 from a combination of observations of H II regions and supernova remnants, deriving  $-0.03 \pm 0.01$  dex kpc $^{-1}$ . Hence, OB 10 is expected to have a metallicity of  $\sim 9.1$  dex, a factor of two greater than the Galactic solar neighbourhood value.

In this paper, William Hershel Telescope (WHT) spectroscopy of OB 10-64 (B0Ia) and OB 10-WR1 (WC6) are combined to reveal the actual metal abundance of this region of M31, plus the properties of WC-type stars in a galaxy similar to our own. Designations are taken from Massey et al. (1986); OB 10-64 has an alternative designation of 41-2265 from Berkhiujsen et al. (1988), while OB 10-WR1 is also known as IT5-19 by Moffat & Shara (1987).

Our observations are presented in Sect. 2. Since the methods used to analyse the spectra of the M31 B-type supergiant and Wolf-Rayet star differ considerably, they are

discussed separately below in Sect. 3 and Sect. 4, with a general discussion presented in Sect. 5.

## 2 OBSERVATIONAL DATA AND REDUCTION

WHT spectroscopy was obtained for OB 10-64 and OB 10-WR1 during Sep–Nov 1998 as part of a programme to observe early-type stars in the spiral galaxies M31 and M33. For OB 10-64 these data were supplemented by Keck I high resolution echelle spectrograph (HIRES) data around the H $\alpha$  region of the spectrum and Hubble Space Telescope (HST) Space Telescope Imaging Spectrograph (STIS) UV spectra.

HD 167264, a Galactic early B-type supergiant, was further observed in September 1998 with exactly the same instrumental setup. For comparison with OB 10-WR1, HD 92809 (WC6) was observed at the Mt Stromlo & Siding Spring Observatory (MSSSO) in Dec 1997. Table 1 summarizes the M31 spectroscopic observations and published photometry.

### 2.1 WHT spectroscopy

The double armed spectrometer ISIS spectroscopy was used to observe OB 10-64 and OB 10-WR1 on the nights of the 28–29 September 1998. The spectrograph slit was positioned so that it included both stars, their separations on the sky being only  $25''$ . Only the blue arm of ISIS was used for the first night, with the R1200B grating and a thinned EEV42-80 CCD (with format  $4096 \times 2048$   $13.5\mu\text{m}$  pixels). On the second night, a beam splitting dichroic was used to feed both the blue and red channels; for the latter, the grating was the R1200R with a TEK CCD used as a detector. For the blue spectra, the unvignetted wavelength range was from approximately  $3985\text{\AA}$  to  $4725\text{\AA}$  with a pixel size of  $0.22\text{\AA}$ ; the corresponding values for the red spectra were  $5650$ – $6400\text{\AA}$  and  $0.4\text{\AA}$ .

Since the above setup was primarily geared towards useful photospheric lines for the B-type supergiant, we missed the crucial WC abundance lines between  $5000$ – $5600\text{\AA}$ . Subsequently, service observations were taken of OB 10-WR1 on November 24<sup>th</sup> 1998, at a lower but sufficient spectral resolution. The R300B and R300R gratings were used in the blue and red arms at dispersions of  $0.9\text{\AA}$  pix $^{-1}$  and  $1.6\text{\AA}$  pix $^{-1}$  covering  $3640$ – $6227\text{\AA}$  and  $6404$ – $9277\text{\AA}$ , respectively.

The CCD frames were reduced to wavelength calibrated spectra using the IRAF reduction system.<sup>†</sup> Standard procedures were used to bias correct and flat field the stellar images. There is considerable background Balmer line emission from the nebular region of OB 10, which can vary over small spatial scales along the slit. Although nebular emission at the sub-pixel level contaminates our stellar Balmer line observations of OB 10-64, the CCD images showed that the H $\delta$  and H $\gamma$  regions were less affected than the H $\alpha$  line.

<sup>†</sup> IRAF is written and supported by the IRAF programming group at the National Optical Astronomy Observatories (NOAO) in Tucson (<http://iraf.noao.edu>).

**Table 1.** Observing log and fundamental properties of the M31-OB 10 targets. UBV photometry is taken from Massey et al. (1986), and  $M_V$  for each star is calculated assuming a distance modulus  $24.47 \pm 0.07$  (Holland 1998, Stanek & Garnavich 1998). The spectral range quoted for the ISIS data is for the unvignetted region; the full blue range was not usable due to the large size of the EEV42-80 CCD and the small entrance window to the ISIS cameras. The resolution is estimated from the width of arc lines measured at the adopted slit-width. The signal-noise-ratio (S/N) per pixel is measured in the continuum after binning by 2 pixels in the spectral direction for the ISIS blue arm, and unbinned data in the red. Note that only 1.0 hour integration was obtained for the red ISIS arm in Sept 1998. The S/N per pixel in the Keck HIRES data is after binning to  $0.3\text{\AA pix}^{-1}$ .

Star	Epoch	Spectral Ranges (Res)	S/N	Exp. Hours	V mag	B-V mag	U-B mag	E(B-V) mag	$M_V$ mag
		Å							
WHT ISIS data:									
OB 10-64	Sep 1998	3985–4725 (0.8)	...	50	4.5	$18.10 \pm 0.04$	$-0.08 \pm 0.08$	$-0.97$	$0.18 \pm 0.08$
OB 10-WR1	Sep 1998	3985–4725 (0.8)	5650–6400 (1.6)	5–15	5.5	$19.32 \pm 0.07$	$-0.56 \pm 0.08$	$-0.45$	$0.18 \pm 0.08$
OB 10-WR1	Nov 1998	3640–6227 (3.5)	6404–9277 (7)	5–15	0.5	...	...	...	...
Keck I HIRES data:									
OB 10-64	Oct 1999	6530–6630 (0.2)	...	~60	4	...	...	...	...
HST STIS data:									
OB 10-64	Oct 1999	1120–1716 (1.5)	...	~20	2.3	...	...	...	...

**Table 2.** Equivalent widths,  $W_\lambda$ , for selected lines of He II, Si III and Si IV in OB 10-64 and HD 167264. These lines are very sensitive to  $T_{\text{eff}}$ , and the similarity of the line strengths indicate that the effective temperatures of the two stars are similar to within 500 K (see Section 3.1). Note that the Si IV line at 4089 is blended with a nearby O II feature, but at this  $T_{\text{eff}}$  the Si IV contribution dominates and the ratio of the line strengths is approximately 4:1. The equivalent widths for OB 10-64 should normally be accurate to 10%; and for HD167264 accuracies are normally 5%.

Species	Wavelength (Å)	$W_\lambda$ (mÅ)	
		OB 10-64	HD 167264
He II	4541	145	110
He II	4686	290	225
Si III	4552	245	225
Si III	4567	240	190
Si III	4574	120	100
Si IV	4089	575	590
Si IV	4116	400	435
Si IV	4654.14	80	80

Further, our spectral resolution is high enough that the important wings of  $H\delta$  and  $H\gamma$  will be unaffected by the background nebulosity. However, there may be residual errors in the cores of the stellar Balmer line profiles. The nebular emission around WR1 is particularly intense and accurate subtraction proved very difficult, however as shown in Figure 9 most of the broader WR features can be modelled while recognising the narrower nebular contamination. The spectra were wavelength calibrated using CuNe+CuAr lamp exposures that interleaved the stellar spectra. Individual stellar exposures were then cross-correlated to search for significant wavelength shifts – none were identified. The spectra were then combined using SCOMBINE and a variety of rejection criteria; the different methods used to combine the data were found to have little effect on the signal-to-noise and the CR rejection success-rate in the final spectra.

Unfortunately conditions in November 1998 prevented an absolute flux calibration for OB 10-WR1. Nevertheless, a relative calibration was achieved, using the spectrophotometric DO white dwarf standard star Feige 110. This star

was observed for 300 sec with an identical setup, immediately prior to OB 10-WR1 and at a similar air mass.

## 2.2 Keck I HIRES and HST STIS spectroscopy of OB 10–64

OB 10-64 was observed with the 10m Keck I telescope, using HIRES on 27th September 1997 and again on the 6/7 October 1999 giving a total of  $4 \times 3600$ s exposures. A  $1.1''$  slit was used giving a resolution of approximately 35 000, yielding a S/N of  $\sim 60$  at  $H\alpha$  after co-addition and binning in the spectral direction to  $0.3\text{\AA pix}^{-1}$ . The CCD echelle spectra were reduced in the standard manner, using the same methods as described in McCarthy et al. (1997). The most difficult task was removing the strong background  $H\alpha$  nebular emission from the stellar spectrum. In fact complete removal proved impossible, and we have left in the residual (negative) nebular  $H\alpha$  line in Figs 6 and 7. This led to an unrecoverable  $0.9\text{\AA}$  region of the spectrum, which is however not critical to our fitting of the much broader stellar  $H\alpha$  profile.

HST spectra were taken with the STIS, as part of an extensive Programme (GO7481) to observe the UV wind-lines of massive blue supergiants in M31 and M33. Two exposures giving a total of 8500s were taken with the FUV-MAMA detector on 1st October 1999. The G140L grating and the  $52 \times 0.2$  arcsec slit aperture were used. The data were pipeline processed, (including wavelength and flux calibration) by the STScI On-The-Fly calibration system<sup>†</sup>. This processes the data with the most up-to-date calibration files, parameters, and software. Further details of the observational material can be found in Table 1.

## 2.3 MSSSO spectroscopy

The Galactic WC6 star HD 92809 was observed with the Double Beam Spectrograph (DBS) at the 2.3m MSSSO on 1997 Dec 24–27. Use of a suitable dichroic permitted simultaneous blue and red observations of HD 92809 covering  $3620$ – $6085\text{\AA}$  (300B) and  $6410$ – $8770\text{\AA}$  (316R), plus  $3240$ –

<sup>†</sup> see <http://www.stsci.edu/instruments/stis>

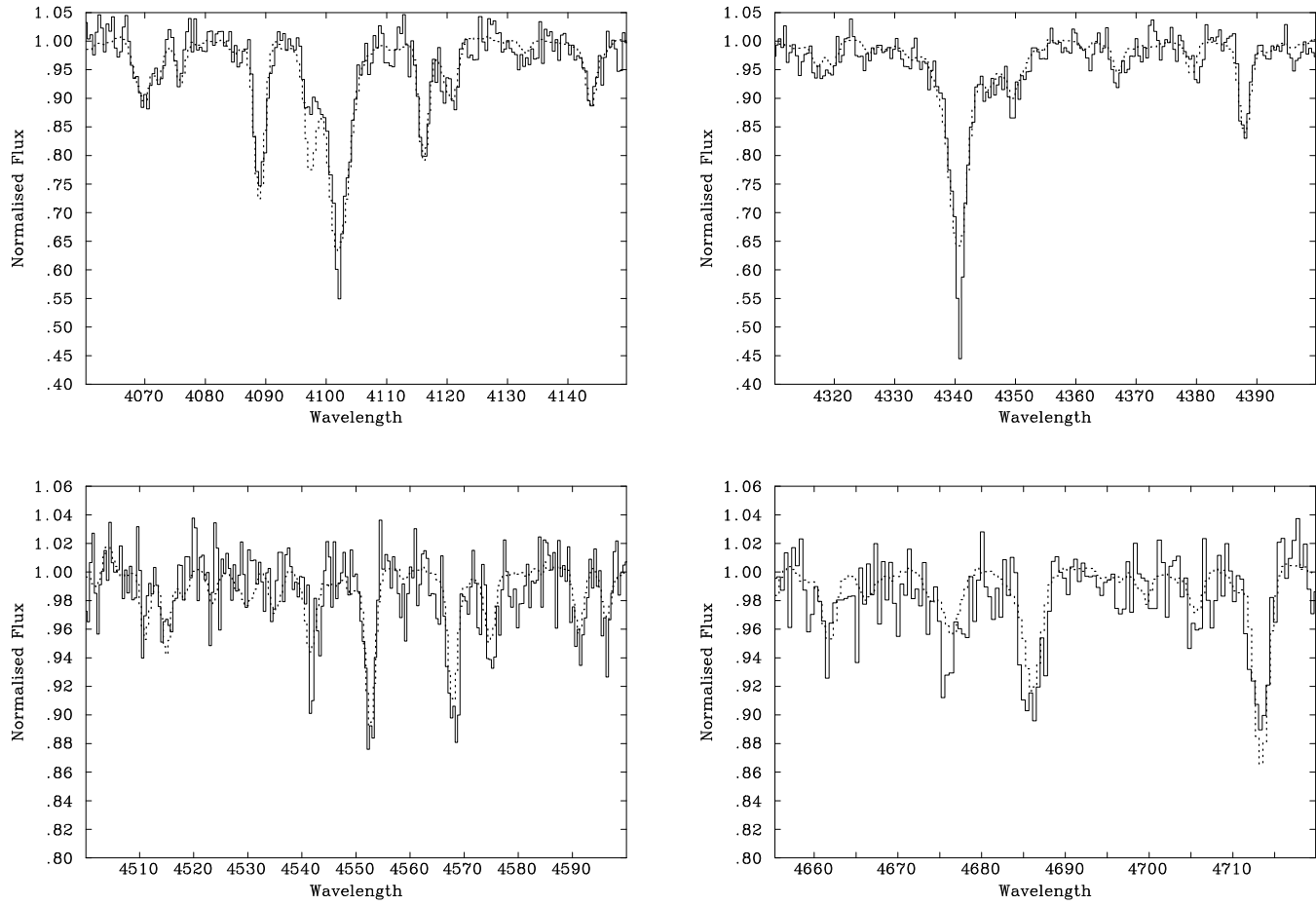


**Figure 1.** Selected spectral regions for OB 10-64 (solid line) and HD 167264 (dotted line), showing temperature sensitive features (He II lines at 4541 and 4686 Å; Si III lines at 4553, 4568 and 4574 Å and Si IV lines at 4089 and 4116 Å) and the surface gravity diagnostics (Balmer lines: H $\delta$  4101 and H $\gamma$  4340 Å). The high quality data of this 18<sup>m</sup> star allow us to identify and measure relatively weak stellar absorption lines due to metals and He I.

4480 Å (600B) and 8640–11010 Å (316R). A 2'' slit and 1752×532 pixel SITe CCDs provided a 2 pixel spectral resolution of  $\sim 5$  Å. Wide slit observations were also obtained for HD 92809 and the HST spectrophotometric standard star HD 60753 (B3 IV) to achieve reliable flux calibration. Atmospheric correction was achieved by observing HR4074 within an air mass of 0.10 from HD 92809. A standard data reduction was again carried out with IRAF.

These observations were supplemented by high resolution (HIRES), International Ultraviolet Explorer (IUE), large aperture, short-(SWP) and long-wavelength (LWP, LWR) ultraviolet observations of HD 92809. These were combined to provide a single high S/N dataset, flux calibrated using the curve obtained by Howarth & Philips (1986). Finally, the spectra were transferred to the STARLINK spectrum analysis program DIPSO (Howarth et al. 1998) for subsequent analysis.

#### 2.4 Photometry, distance and reddening to M31

The published photometry of both stars (from Massey et al. 1986) is provided in Table 1. Assuming  $(B-V)_0 = -0.26$  for a B0 Ia atmosphere (Deutschman et al. 1976), we estimate an interstellar reddening of  $E(B-V)=0.18$  mag to-

wards OB 10-64. Massey et al. (1995) have estimated the mean reddening toward the massive stars with spectroscopically confirmed types in OB 10 and OB8 + OB9, deriving a value of  $E(B-V)=0.16 \pm 0.02$ . The reddening directly towards OB 10-64 is hence compatible with the mean value for the region. Assuming the distance of Holland (1998) to M31 of  $783 \pm 30$  kpc implies  $M_V = -6.93 \pm 0.42$  for OB 10-64 (from the errors quoted in Table 1). We discuss the implications of this in terms of wind and evolutionary models in Section 5.

Our HST STIS data was combined with existing archive FOS and GHRS data to give a flux distribution from 1120–3300 Å. For the value of  $E(B-V)=0.18$ , the de-reddened HST/FOS flux distribution for OB 10-64 matches theoretical models for  $\lambda \geq 2000$  Å but shows a noticeable drop at shorter wavelengths, possibly indicating a different far-UV reddening law to the Galactic case (Seaton 1979). Bianchi et al. (1996a) investigated the extinction in M31 using the HST/FOS data for OB 10-64 and additional M31 OB stars and concluded that the 2175 Å bump is weak or absent in M31. The slope of the extinction curve was consistent with the Galactic curve, but the low reddening of their M31 target stars prevented strong constraints being placed on the exact shape of this extinction curve. We have briefly re-

investigated this issue using a slightly different procedure, following Fitzpatrick (1986) in using other B-type supergiants in the LMC as the comparison stars. We chose Sk-67 108 (B0 Ia) and Sk-69 276 (O9–B0 Ia) as the comparison stars on the basis of the morphology of their UV spectra compared to OB 10-64. These two stars have essentially little or no internal LMC extinction and the  $E(B-V)$  values (0.06 and 0.10 respectively) reflect the reddening from intervening Galactic material. This Milky Way extinction is similar to what we expect for OB 10-64. Using these two stars and OB 10-64 we derive a mean M31 extinction law, which confirms the lack of a 2175Å feature in M31, similar to the SMC (Prevot et al. 1984). We find a slope for M31 which is marginally shallower than the SMC, but steeper than that of the Milky Way. A linear fit of  $E(\lambda-V)/E(B-V)$  versus  $\lambda^{-1}$  ( $\mu^{-1}m$ ) gives a slope of approximately 1.8 for M31; compared with approximately 2.2 for the SMC. This analysis suggests that the far-UV extinction in M31 is greater than that predicted by the Galactic extinction law, and that there is a lack of the 2175Å bump. However this should be treated with some caution as we have only one star available here, and it is only lightly reddened by dust in M31 itself. Ideally stars with higher M31 extinction (or preferably a range in values) are needed to investigate the relationship fully.

For the Wolf-Rayet star, broad-band Johnson photometry are (differentially) contaminated by strong emission lines. Consequently, the Massey et al. (1986) V-band magnitude for OB 10-WR1 will overestimate the true continuum flux, and the observed B-V colour does not permit the determination of interstellar reddening. Therefore, we assume an identical reddening to that derived above for OB 10-64 and estimate a Smith narrow  $v$ -band magnitude for OB 10-WR1 as follows. We have convolved our WHT spectra of OB 10-WR1 and OB 10-64 with a Johnson V-band filter, revealing  $\Delta V=1.25$  mag, in excellent agreement with 1.22 from Massey et al. (1986). Applying the  $v$ -band filter to the spectrum of OB 10-WR1 yields  $(v-V)=0.35$  mag, so we estimate  $v=19.67$  mag. This agrees well with the narrow-band 4752Å continuum magnitude of 19.6 quoted by (Massey & Johnson 1998) for OB 10-WR1. Taking the above distance and adopting a reddening of  $E(B-V)=0.18$  implies  $M_v=-5.4\pm0.4$  mag. This result is significantly different from the mean absolute magnitudes of  $M_v=-3.7$  mag and  $-4.8$  mag for respectively, Galactic WC6 and WC7 stars (e.g. Smith et al. 1990).

## 2.5 Spectral types

While spectral typing is often neglected when carrying out quantitative atmospheric and wind analysis of massive stars, we quote our revised types to allow the stars to be put into context with other morphological work. Humphreys et al. (1990) and Massey et al. (1995) gave a spectral type of B1 I for OB 10-64 based on spectral data of 2–3.5Å resolution and moderate signal-noise, while Bianchi et al. (1996b) presented HST ultraviolet spectroscopy of OB 10-64, suggesting approximately B0.5 Ib. From our higher quality optical and UV spectra we have adjusted the spectral type slightly to B0 Ia (see also Fig. 4). Meanwhile, Massey et al. (1986) classified OB 10-WR1 as a WC6–7 star, which Moffat & Shara (1987) revised to WC6+neb!. Our high quality spectrum

confirms the WC6 classification using either the Smith et al. (1990) or Crowther et al. (1998) schemes, plus the strong nebular contamination.

## 3 B-TYPE SUPERGIANT ANALYSIS

The non-LTE model atmosphere techniques have been described in detail by McErlean et al. (1999 - hereafter designated as MLD) and here we only provide a summary. A grid of non-LTE model atmospheres was generated using the code TLUSTY (Hubeny 1988) for effective temperatures,  $T_{\text{eff}}$ , upto 35 000 K and logarithmic gravities from  $\log g=4.5$  down to near the Eddington stability limit. Models were calculated for two helium fractions, viz.  $y=0.09$  (solar) and  $y=0.20$ , where  $y=N[\text{He}]/N[\text{H}+\text{He}]$ . The models omit a number of physical processes, including metal line-blanketing and wind effects. Furthermore, the assumption of a plane-parallel geometry may be of limited validity for the low gravity objects considered here. The consequences of these omissions have been discussed in MLD.

The line formation calculations were performed using the codes DETAIL (Giddings 1981) and SURFACE (Butler 1984). Microturbulent velocities, which are close to the speed of sound, have previously been found for B-type supergiants. Therefore, in the calculation of line profiles, microturbulence has been included as an extra free parameter. Metal ion populations and line-profiles were calculated using mainly the atomic data of Becker & Butler (1988, 1989, 1990). Such calculations explicitly include the effects of the relevant ions on the radiation field. However they do not include the effects of line and continuum blanketing from other metals.

Significant difficulties were encountered in running DETAIL particularly for the silicon model ion but also for some other species. These difficulties occurred mainly at the lowest gravities for effective temperatures greater than  $\sim 25\,000$  K. Examination of the line profiles indicated that this was caused by either emission or ‘filling in’ of the profiles. Indeed the DETAIL calculations normally showed an overpopulation of the relevant ionic upper levels coupled with large photoionization rates (and subsequent cascades). MLD postulated that the emission was an artefact of their exclusion of line blanketing which leads to an overestimate of the UV flux and hence of the photoionization rates - further discussion of these problems can be found in their paper, while their implications for the current dataset are discussed below.

### 3.1 Atmospheric parameters

A comparison of the spectra of OB 10-64 and HD 167264 indicates that these stars have very similar, if not identical, atmospheric parameters within the errors of our methods. This is illustrated in Fig. 1, where four spectral regions are shown for the two stars. These regions contain diagnostics of the atmospheric parameters as discussed below:

**Effective temperature:** As discussed by MLD, both the strength of the He II features and the relative strengths of lines due to Si III and Si IV can be used to estimate the effective temperature for spectral types near B0. The former

is an excellent diagnostic with a change of effective temperature of 2000K leading to changes in the He II equivalent widths of a factor of two or three; additionally MLD found that the He II line at 4541Å appeared to be well modelled by the non-LTE calculation. In Fig. 1, two He II lines at 4541Å and 4686Å are shown; their strengths seem very similar in the two stars. This is confirmed by the observed equivalent widths (see below for details of the procedures used to estimate these values) summarized in Table 2. Although the line strengths are approximately 20-30% larger for OB 10-64, this would correspond to a change in effective temperature of less than 500K, such is the sensitivity of the line strength to temperature in this  $T_{\text{eff}}$  range.

Lines due to Si III (at approximately 4553, 4568 and 4574Å) and Si IV (at 4089 and 4116Å) are also shown in Fig. 1. Again the agreement is excellent as is confirmed by the estimates of the equivalent widths listed in Table 2. For OB 10-64, the Si III lines are marginally enhanced and the Si IV lines marginally weakened compared with the standard star. This would imply that OB 10-64 had a lower effective temperature, in contrast to the He II lines that implied that this star was hotter. However, again the differences are marginal and would imply a temperature difference between the two stars of less than 500K.

**Surface gravity:** The profiles of the Balmer lines are useful diagnostics of the surface gravity and in Fig. 1, the H $\gamma$  (at 4340Å) and H $\delta$  (at 4101Å) are shown. In the line wings (which have the greatest sensitivity to the gravity), the agreement between the two stars is excellent and imply that the gravities (assuming that the stars have similar effective temperatures) differ by less than 0.2 dex; the major uncertainty arises from the difference in S/N of the observational data for OB 10-64 compared to the bright standard. In the line cores, there are significant differences but this is likely to be due to different amounts of rotational or macroturbulent broadening rather than a difference in the surface atmospheric parameters. Additionally for the OB 10-64 spectra there were significant amounts of background emission from the host galaxy as discussed in the previous section; the discrepancies may in part reflect the difficulty in subtracting this background emission accurately.

Hence we conclude that within the observational uncertainties, these two stars have the same atmospheric parameters. MLD deduced an effective temperature of 29000K and a logarithmic gravity of 3.1 dex for HD 167264 from the optical spectroscopy of Lennon et al. (1992; 1993). We have used our better quality ISIS observations to check these results using the same diagnostics as MLD, namely the He II lines for effective temperature and the Balmer line profiles for the gravity. At these relatively high effective temperatures, the non-LTE calculations of the Si III spectrum (and to a lesser extent the Si IV spectrum) becomes problematic (see MLD for details) and hence these lines were not be considered.

The observed and theoretical spectra are shown in Fig. 2, with the latter having been convolved with a Gaussian profile with a FWHM of 0.80Å to allow for instrumental, rotational and macroturbulent velocity broadening. In general the agreement is good, apart from the He II line at 4541Å, where the wings of the theoretical profile appear to be too strong. However even for this case, a decrease of only 1000K would lead to a theoretical profile that is significantly weaker than the observed. Hence we conclude that the atmospheric

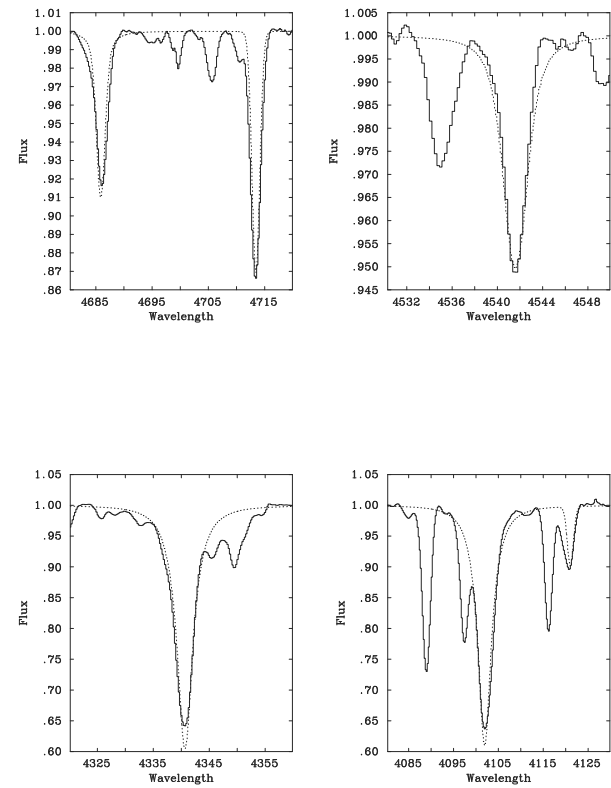


**Figure 2.** Observed (solid line) and non-LTE (dotted line) spectra for HD 167264. The upper two panels show the He II lines at 4541Å and 4686Å which are diagnostics of the effective temperature. The lower two panels show the gravity sensitive Balmer lines, H $\delta$  and H $\gamma$ . Excellent agreement is found between the line profiles and strengths.

parameters of MLD are reliable and adopt them for both HD 167264 and OB 10-64. Additionally, MLD found that a microturbulent velocity of 10 km s $^{-1}$  was appropriate for the Si III features in B-type supergiant spectra. They also noted that the O II spectra implied a higher microturbulent velocity – a result found independently by Vrancken et al. (1999) for early-B-type giants. Here we adopt a microturbulent velocity of 10 km s $^{-1}$  for both stars but will consider below the effect of a larger value being appropriate.

### 3.2 Chemical composition

The choice of a standard with atmospheric parameters effectively identical to those for OB 10-64 simplifies the abundance analysis. Our procedure was as follows. Firstly metal line absorption features were identified in the spectra of OB 10-64. For marginal features, the spectrum of HD 167264 was used as a template and guide. The equivalent widths of the features were estimated in both stars by non-linear least squares fitting of single or multiple Gaussian absorption profiles to the normalised spectra. Normally both the positions and widths of the Gaussian profiles were allowed

to vary. However for multiplets the relative wavelength separations were fixed, while for marginal features in OB 10-64, the widths were set to the mean value found for well observed lines. The equivalent widths are listed in Table 3, apart from those for silicon, which are in Table 2; all estimates have been rounded to the nearest 5 mÅ.

For most species, these equivalent widths were analysed using the non-LTE grids of MLD and the atmospheric parameters discussed above. As well as absolute abundance estimates a line-by-line differential analysis was also undertaken. For the N III spectrum and one Si IV line, non-LTE calculations were not available and LTE methods were used; in these cases, the absolute abundance estimates should be treated with caution. However, the similarity in both the observed line strengths and inferred atmospheric parameters for OB 10-64 and HD 167264 imply that the differential abundance estimates should be reliable. This was confirmed by re-analysing the O II line spectrum using an LTE technique, where the *differential* abundances agreed with the non-LTE estimates to normally within 0.01 dex. Both the absolute and differential abundance estimates are summarized in Table 5, together with the number of features used and whether an LTE or non-LTE formulation was adopted. Note that the latter information is replicated in Table 3, together with information on which features were included in the abundance analysis. The error estimates in Table 5 are unweighted standard deviations of the samples; where a significant number of features were measured, the uncertainty in the means should be smaller.

### 3.3 Photospheric abundances of OB 10-64

The atmospheric parameters and chemical composition of OB 10-64 appear to be very similar to those of HD 167264. Below, we discuss the abundances of individual elements in detail:

**Helium:** The helium abundance in OB 10-64 has not been determined explicitly. This was because most of the He I non-diffuse features were either badly blended with metal lines (e.g. the line at 4121Å) or weak (the lines at 4169Å and 4437Å). The only well observed non-diffuse feature is the triplet line at 4713Å and as can be seen from Fig. 1, the profiles for the two stars are very similar. Additionally the moderate quality of the observational data for OB 10-64 would make reliable profile fitting of the helium diffuse lines difficult. However in Fig. 3, selected diffuse helium lines are shown for the two stellar spectra. In general, agreement is excellent and we conclude that within the observational uncertainties the helium abundances in the two objects are similar.

**Carbon:** The carbon abundances are based on a single weak feature (the 4267Å doublet) which is of similar strength in each star. MLD have commented on the fact that the line appears difficult to model properly with the non-LTE techniques that we use here. Even in B-type dwarfs, calculation of this transition is problematic in both LTE and non-LTE. Hence while the absolute abundance estimates should be treated with considerable caution, the similarity in line strength points to both stars having similar C photospheric abundances.

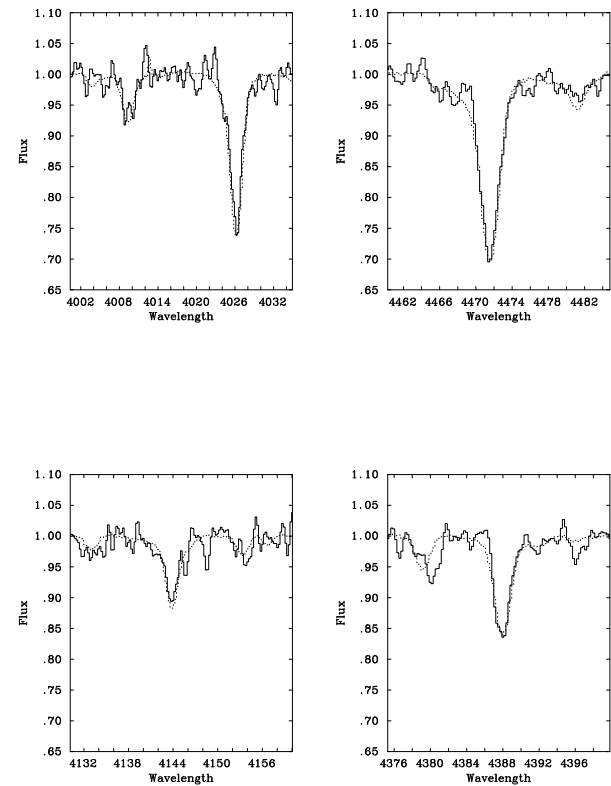


**Figure 3.** Selected spectral regions for OB 10-64 (solid line) and HD 167264 (dotted line), showing He I diffuse lines at 4009 and 4026Å, 4471Å, 4143Å, 4387Å.

**Nitrogen:** This element is particularly important as it provides an excellent diagnostic for the mixing of nucleosynthetically processed material from the stellar core to the surface. Hence, a search was made for lines of both N II and N III in the spectrum of OB 10-64. Unfortunately all the detections were marginal and the corresponding line strengths should be treated with caution. The single N II line implies that the two stars have similar nitrogen abundances while the four N III lines implies that OB 10-64 is depleted by approximately 0.2 dex. However it should be noted that the theoretical N III line strengths are very sensitive to the adopted effective temperature, which coupled with the observational uncertainties, implies that this difference is probably not significant.

**Oxygen:** This is the best observed species with 13 lines being analysed. The oxygen abundances in the two stars are very similar as can be seen from the absolute abundance estimates. It is encouraging that the standard error for the differential abundance is significantly smaller implying that the use of a differential method is indeed removing some sources of systematic error. Assuming that the remaining errors are distributed normally, the estimated uncertainty in the mean differential abundance would be reduced to ap-

**Table 5.** Absolute and differential abundances for OB 10-64 and HD 167264. Where more than one feature was measured for a given species (as denoted by  $n$  = number of available lines), the unweighted mean is quoted with the error being the standard deviation of the sample. The method of line formation calculation is noted, and for further information see the text. For reference we quote the abundances in solar neighbourhood B-type stars from Gies & Lambert (1992) for all elements apart from Mg which is from Kilian (1994)

Ion	$[\frac{X}{H}]$		$\Delta[\frac{X}{H}]$	$n$	Method	Solar B-star abundances
	OB 10-64	HD 167264				
C II	7.83	7.78	+0.05	1	non-LTE	8.20
N II	7.96	7.90	+0.06	1	non-LTE	7.81
N III	8.40±0.07	8.60±0.27	-0.20±0.30	4	LTE	7.81
O II	8.69±0.34	8.62±0.23	+0.07±0.15	13	non-LTE	8.68
Mg II	7.36	7.30	+0.06	1	non-LTE	7.45
Si III	7.54±0.18	7.34±0.12	+0.20±0.10	3	LTE	7.58
Si IV	7.7:	7.8:	-0.16	2	see text	7.58

proximately  $\pm 0.02$  and hence there is marginal evidence for a slight enhancement in OB 10-64.

**Magnesium:** The estimates are again based on a single feature but the two stars appear to have similar abundances.

**Silicon:** The Si III lines were analysed using both non-LTE and LTE methods. The former leads to higher absolute estimates but a similar differential abundance as for the LTE calculations. As discussed by MLD, the non-LTE profiles of the Si III lines show some emission in their wings in this temperature regime; this is probably an artifact of the lack of line blanketing in the calculations. Hence in Table 5 the LTE results are summarized but the absolute abundance estimates should be treated with caution. The differential abundance implies a small silicon enhancement in OB 10-64 in contrast to that found from the two Si IV lines. The latter result should also be treated with some caution as the analysis of one of the Si IV lines was undertaken in LTE (it was not included in the non-LTE model ion), which will make the absolute abundance estimates particularly unreliable. Additionally the theoretical line strengths are extremely sensitive to the adopted effective temperature with, for example, a change of less than 1000K being sufficient to eliminate the discrepancy. Hence we believe that the Si III differential abundance is the more reliable.

Despite the difficulties for individual ions discussed above, we believe that the differential abundance estimates should be generally reliable. This reflects the similar atmospheric parameters and metal line equivalent widths for the two stars. The former ensures that the method of analysis (LTE or non-LTE) is relatively unimportant and indeed we confirmed this by re-analysing the O II equivalent widths using LTE methods. Additionally the similarity in line strengths makes the choice of the microturbulent velocity relatively unimportant provided it is the same in both stars; for example, re-analysing the metal line spectra with a microturbulent velocity of  $15 \text{ km s}^{-1}$  changed the differential estimates by less than 0.05 dex.

### 3.4 Wind Analysis and Stellar Wind Momentum

OB 10-64 is an ideal object to test the validity of the concept of the wind momentum – luminosity relationship. It

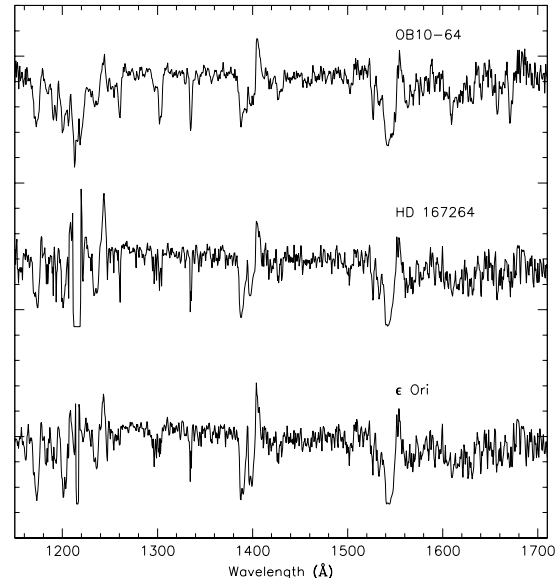


**Figure 4.** A compilation of galactic IUE spectra of two B0 Ia Galactic stars and the STIS spectra of OB 10-64.

has a well determined chemical composition comparable to the solar neighbourhood and an equally well determined effective temperature and gravity. The reddening is moderate and the absolute magnitude follows from the distance to M31 (see Table 1). Using a non-LTE model atmosphere code with the corresponding effective temperature and gravity we can calculate the emergent stellar flux and determine the stellar radius from the absolute V-band magnitude (see Kudritzki 1980). We obtain a radius of  $R = 34R_{\odot}$ . This means that OB 10-64 has stellar parameters very similar to the galactic object HD 37128 ( $\epsilon$  Ori), which has been investigated recently by Kudritzki et al. (1999) in their study of the wind momentum – luminosity relationship of galactic A- and B-supergiants. We therefore expect both objects to have comparable wind momenta. HD167264, the Galactic comparison object for the abundance study in this paper, has a very uncertain distance (and, therefore, radius and luminosity). From the similarity of the spectra we can only

assume that its luminosity must be comparable to OB 10-64 and HD 37128.

An inspection of Fig. 4 immediately indicates (albeit in a qualitative manner) that the stellar wind properties of the three objects cannot be very different. For the quantitative wind analysis of OB 10-64 we proceed exactly in the same way as described by Kudritzki et al. (1999). First, we measure the terminal velocity  $v_\infty$  of the stellar wind from radiative transfer fits of the strong UV resonance lines of N V, C IV and Si IV using the method developed by Haser (1995) (see also Haser et al. 1995, Haser et al. 1998, Lamers et al. 1999). This is similar to the technique applied by Howarth et al. (1997). The fit yields  $v_\infty = 1650 \text{ km s}^{-1}$  for both OB 10-64 and HD167264 (see Fig. 5), which is very close to the value of  $1600 \text{ km s}^{-1}$  found for HD 37128.

Subsequently, the mass-loss rate  $\dot{M}$  can be obtained from a fit of the observed line profile of H $\alpha$ . This requires a non-LTE unified model atmosphere analysis incorporating the stellar wind and spherical extension (Kudritzki et al. 1999). Assuming a radius of  $34 R_\odot$  and a terminal velocity of  $v_\infty = 1650 \text{ km s}^{-1}$ , we calculated a sequence of unified models with different mass-loss rates. Fig. 7 gives an idea of the accuracy of the line profile fit, which is somewhat restricted due to the central contamination by the H II-region emission. Despite this, a reasonable determination of the mass-loss rate is certainly possible. Values as low as  $1.0 \times 10^{-6} M_\odot \text{ yr}^{-1}$  can clearly be ruled out together with values above  $1.75 \times 10^{-6} M_\odot \text{ yr}^{-1}$ . We adopt  $1.6 \times 10^{-6} M_\odot \text{ yr}^{-1}$  as the model which gives the best compromise fit in Fig. 7. This means that OB 10-64 has a slightly lower mass-loss rate than HD 37128 ( $2.5 \times 10^{-6} M_\odot \text{ yr}^{-1}$ , Kudritzki et al. 1999). The modified stellar wind momentum  $\log(\dot{M} v_\infty (R/R_\odot)^{0.5})$ , which is expected to be a function of luminosity only, is 28.98 (in cgs-units) compared to 29.15 for HD 37128. Fig. 8 compares the modified wind momenta of OB 10-64 and of all the galactic early B-supergiants studied by Kudritzki et al. (1999). Within the intrinsic scatter of the wind momentum – luminosity relationship the agreement is excellent. This is the first direct demonstration that the concept of the WLR works for objects of this spectral type (i.e. early B-types) outside our own Galaxy.

## 4 WOLF-RAYET ANALYSIS

### 4.1 Technique

We use the non-LTE code of Hillier & Miller (1998) which iteratively solves the transfer equation in the co-moving frame subject to statistical and radiative equilibria in an expanding, spherically symmetric and steady-state atmosphere. Relative to earlier versions of this code (Hillier 1987, 1990), two major enhancements have been incorporated, of particular relevance to WC-type stars, namely (i) line blanketing, (ii) clumping.

Our analysis of OB 10-WR1 follows a similar method to that recently applied to Galactic WC stars by Hillier & Miller (1999). Specific details of the (extremely complex) model atoms used here for our quantitative analysis are provided in Dessart et al. (2000), together with information on the source of atomic data used for He I-II, C II-IV, O II-VI, Si IV and Fe IV-VI. We use an identical (slow) form of the

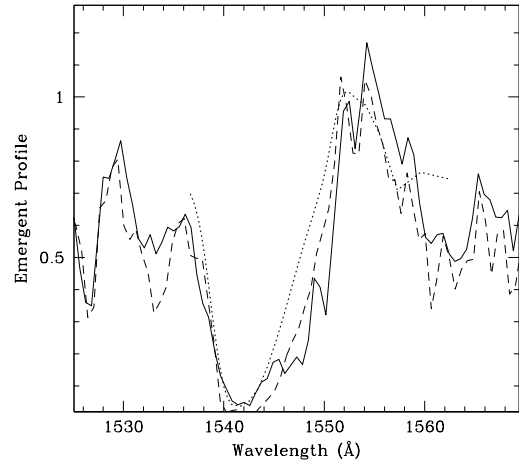


**Figure 5.** The wind analysis fit (dotted line) for  $v_\infty$  shown for the C IV line only. OB 10-64 is the solid line and HD167264 is the dashed. The HD167264 high-resolution IUE spectra has been degraded to the STIS resolution. A  $v_\infty=1650 \text{ km s}^{-1}$  is found.

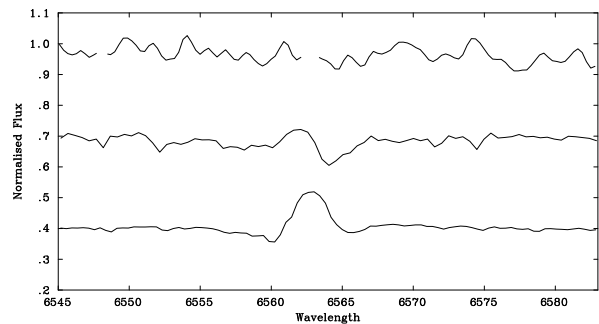


**Figure 6.** Comparison between the H $\alpha$  profiles of OB 10-64 (upper) and HD167264 (middle) and HD37128 (lower). The Keck I HIRES data of OB 10-64 has been convolved with a Gaussian to yield the same resolution as the spectra of HD167264 and HD37128 (see Lennon et al. 1993 for details of Galactic star observations), and re-binned to a pixel size of  $0.3 \text{ Å}$ . The nebular lines in OB 10-64 which could not be subtracted properly have been snipped out. The profiles of the three stars are qualitatively very similar indicating similar wind characteristics. Further, the differential photospheric analysis is not compromised by different wind properties of OB 10-64 and HD167264.

velocity law, such that acceleration is modest at small radii, but continues to large distances. We assume that the wind is clumped with a volume filling factor,  $f$ , and that there is no inter clump material. Since radiation instabilities are not expected to be important in the inner wind we parameterise the filling factor so that it approaches unity at small velocities. Clumped and non-clumped spectra are very similar, except that line profiles are slightly narrower with weaker electron scattering wings in the former. Although non-clumped models can be easily rejected (Hillier & Miller 1999), be-

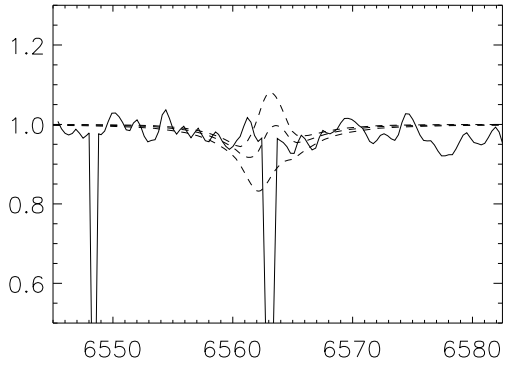


**Figure 7.** The wind model fit to the Keck I HIRES spectra of H $\alpha$  assuming the parameters outlined in Table 4. The sharp absorption-like features reflect the difficulty or reliably subtracting the background nebular lines (H $\alpha$  and [N II] 6548.1Å), and these parts of the stellar spectra are unrecoverable. Despite this, the H $\alpha$  stellar wind profile can be fitted quite accurately. Three NLTE unified model calculations for  $\dot{M} = 1.00, 1.50, 1.75 \times 10^{-6} M_{\odot}/\text{yr}$  are shown as dashed curves.

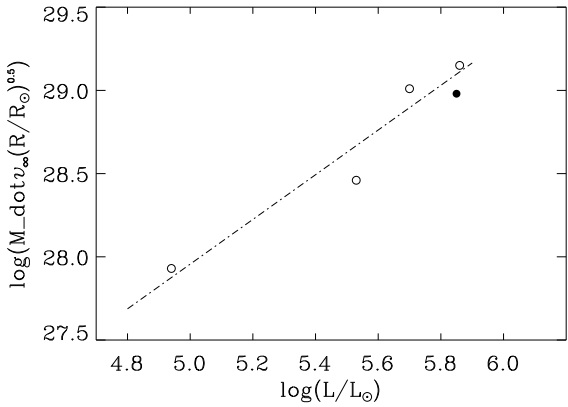


**Figure 8.** Modified Wind Momentum of OB 10–64 (solid) compared with the galactic supergiants of early B-type spectral type in Kudritzki et al. (1999) (open circles). The regression curve is a fit to the galactic objects only.

cause of the severe line blending in WC winds  $\dot{M}/\sqrt{f}$  is derived by our spectroscopic analysis, rather than  $\dot{M}$  and  $f$  independently.

## 4.2 Spectroscopic analysis of OB 10–WR1

As usual, a series of models were calculated in which stellar parameters ( $T_*$ ,  $\log L/L_{\odot}$ ,  $v_{\infty}$ ,  $\dot{M}/\sqrt{f}$ , C/He, O/He) were adjusted until the observed ionization balance, line strengths, widths, and absolute  $v$ –band flux were reproduced. Because of the (substantial) effect that differing mass-loss rates, temperatures and elemental abundances have on the emergent spectrum, this was an iterative process.

The wind ionization balance is ideally selected on the

basis of isolated optical lines from adjacent ionization stages of carbon (e.g. C III  $\lambda 6740$ /C IV  $\lambda 7700$ ) and/or helium (He I  $\lambda 5876$ /He II  $\lambda 5412$ ). In practice, this was difficult to achieve because of the severe blending in WC winds, so our derived temperature should be treated as approximate. Current spectroscopic models fail to reproduce the absolute and relative strength of the WC classification lines at C III  $\lambda 5696$  and C IV  $\lambda\lambda 5801\text{--}12$  (see Hillier & Miller 1998 and Dessart et al. 2000). As in other recent spectroscopic studies of WC stars, He II  $\lambda 5412$ /C IV  $\lambda 5471$  were selected as the principal C/He diagnostic since the relative strength of these features are insensitive to differences of temperature or mass-loss rate. Oxygen abundances were impossible to constrain, since the principal diagnostic region spans  $\lambda\lambda 2900\text{--}3500$  (Hillier & Miller 1999). Consequently, we adopt C/O $\sim 4$  by number as predicted by stellar evolutionary models (Schaller et al. 1992). Based on results obtained for OB 10–64 in Sect. 3, we shall adopt solar abundances for Si and Fe.

As discussed by Hillier & Miller (1998), many weak spectral features sit upon the continuum so that ideally one would wish to compare synthetic models with fluxed spectroscopy. Since absolute fluxes are unavailable for OB 10–WR1, we have instead rectified the dataset, taking care to use as few ‘continuum’ regions as possible.

Our ISIS spectroscopic data of OB 10–WR1 is shown in Fig. 9. Overall, the spectrum is reasonably well reproduced by our model, except that C III  $\lambda 5696$  and C IV  $\lambda\lambda 5801\text{--}12$  are too weak. Nebular emission lines are prominent in the observed spectrum, and contaminate the He II  $\lambda 6560$  and C III  $\lambda 6740$  stellar lines. We find  $T_* \sim 75$  kK,  $\log L/L_{\odot} = 5.68 \pm 0.16$ ,  $v_{\infty} \sim 3000 \text{ km s}^{-1}$  and  $\dot{M}/\sqrt{f} \sim 10^{-4.3} M_{\odot}/\text{yr}^{-1}$ , with C/He $\sim 0.1$  by number, from He II  $\lambda 5412$ /C IV  $\lambda 5471$ , despite the low S/N achieved in this region from a single 30 minute ISIS exposure. The wind performance number of OB 10–WR1 is  $\dot{M}v_{\infty}/(L/c) \sim 14$  for our assumed  $f=0.1$ .

In order to better constrain the stellar parameters of OB 10–WR1, one would require UV spectroscopy with HST/STIS to permit a reliable reddening determination (the chief source of uncertainty in  $\log L/L_{\odot}$ ),  $v_{\infty}$  via P Cyg resonance lines, and oxygen abundances from the near-IR diagnostics. For  $E(B-V)=0.18$ , the expected UV continuum flux from OB 10–WR1 is  $2 \times 10^{-16} \text{ erg cm}^{-2} \text{ s}^{-1} \text{ \AA}^{-1}$  at 3000Å, or  $1 \times 10^{-15} \text{ erg cm}^{-2} \text{ s}^{-1} \text{ \AA}^{-1}$  at 1500Å, assuming a standard Galactic extinction towards OB 10 (though see Sect. 2.4).

## 4.3 Quantitative comparison with HD 92809 (WC6)

How do the parameters of OB 10–WR1 compare with WCE counterparts in other galaxies? Amongst Galactic WC6 stars, only HD 92809 (WR23) and HD 76536 (WR14) are moderately reddened and lie at established distances (Koesterke & Hamann 1995). Since high quality flux calibrated spectroscopy of HD 92809 are available to us (Sect. 2), we now carry out an identical analysis of it, permitting a quantitative comparison to be carried out. Although numerous Galactic WCE stars have been studied by Koesterke & Hamann (1995), including HD 92809, the inclusion of line blanketing and clumping into models has a major effect on the stellar luminosity and wind density, just

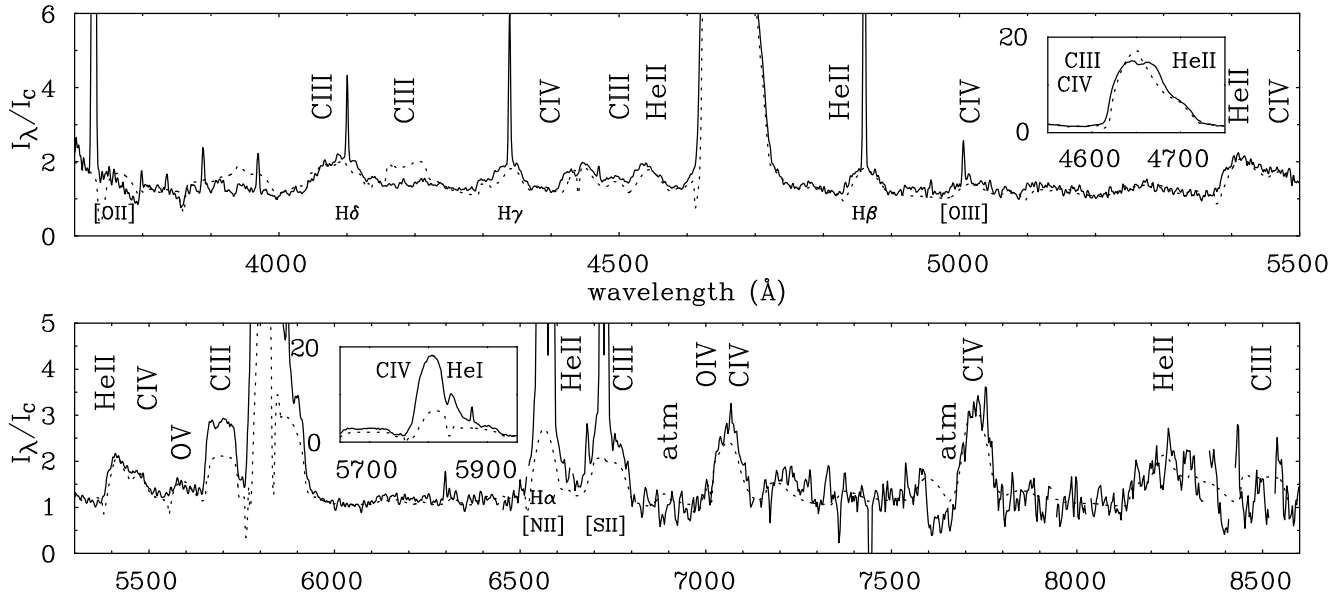


**Figure 9.** Comparison between rectified WHT/ISIS spectroscopy of M31-OB 10-WR1 (solid) and our synthetic model (dotted). Strong nebular emission lines severely contaminate the He II  $\lambda 6560$  and C III  $\lambda 6740$  emission lines, while atmospheric features in the far-red have not been removed.

tifying the need for a re-evaluation of its properties (Dessart et al. 2000).

HD 92809 lies in the Car OB1 association, at a distance of 2.63 kpc, with a narrow  $v$ -band Smith magnitude of 9.71 mag. Our spectral synthesis of HD 92809, using methods identical to those described above, indicates a reddening of  $E(B-V)=0.50$  mag (Koesterke & Hamann (1995) obtained  $E(B-V)=0.38$ ), such that  $M_v=-4.08$  mag, substantially lower than OB 10-WR1 ( $M_v=-5.4\pm0.4$  mag). We adopt  $v_\infty=2280$  km s $^{-1}$  for HD 92809 following the UV analysis by Prinja et al. (1990), also somewhat lower than OB 10-WR1. The measured emission equivalent widths of selected lines in the optical spectra of OB 10-WR1 and HD 92809 are listed in Table 6. In general, HD 92809 has similar line equivalent widths to OB 10-WR1, except that the He II  $\lambda 5412$ /C IV  $\lambda 5471$  ratio is much smaller, suggesting a higher carbon abundance. Single WC stars appear to show remarkably uniform emission equivalent widths at each spectral type, oblivious of their stellar parameters or chemistry. For example, Conti & Massey (Conti & Massey 1989) measured C IV  $\lambda 5801-12$  equivalent widths in the range 440–1150 Å for (apparently) single Galactic WC6 stars. Therefore, we can have confidence that OB 10-WR1 is also single.

Our spectroscopic analysis was repeated for HD 92809, with our final UV and optical synthetic spectrum compared with observations of HD 92809 in Fig. 10 (de-reddened by  $E(B-V)=0.50$  mag following the reddening law of Seaton (1979)). Overall, the comparison is excellent for line strengths, shapes, as is the match to the continuum distribution throughout the spectrum. The number of line features that are poorly reproduced is small, and again includes C III  $\lambda 5696$ , C IV  $\lambda\lambda 5801-12$ .

For HD 92089, we derive the following stellar parameters:  $T_*=75$  kK,  $\log L/L_\odot=5.3$ , and  $\dot{M}/\sqrt{f} \sim$

$10^{-4.8} M_\odot \text{yr}^{-1}$ . Fits to He II  $\lambda 5412$  and C IV  $\lambda 5471$  imply C/He $\sim 0.3$  by number, confirming the higher carbon abundance expected from their line ratio. Near-UV oxygen diagnostics are well matched for HD 92809 with an assumed C/O=4 number ratio. As discussed previously by Hillier & Miller (1999) and Dessart et al. (2000), the inclusion of line blanketing into WC models significantly increases stellar luminosities relative to previous studies – taking the higher reddening into consideration, blanketing increases the luminosity for HD 92809 by  $\sim 0.25$  dex relative to Koesterke & Hamann (1995). We confirm the previously derived stellar temperature and carbon abundance for HD 92809. A clumping factor of  $f=0.1$  reduces the global mass-loss rate by  $\sim 3$ , so that the overall effect of our study is to decrease the wind performance number for HD 92809 to 8 from 108 (Koesterke & Hamann 1995). This dramatically alleviates the Wolf-Rayet ‘momentum problem’, such that multiple scattering of photons in their highly stratified atmospheres *may* be able to account for their mass-loss properties via radiatively driven wind theory.

## 5 DISCUSSION

### 5.1 Comparison of the Galactic and M31 B-supergiants

The differential analysis of the B-types implies that the two stars appear to have very similar chemical compositions. There is some marginal evidence for a small metal enhancement in OB 10-64 but this could, for example, just be an artifact of an overestimation of its equivalent widths from the lower quality spectroscopic data. We believe the differential oxygen abundance to be particularly sound given the

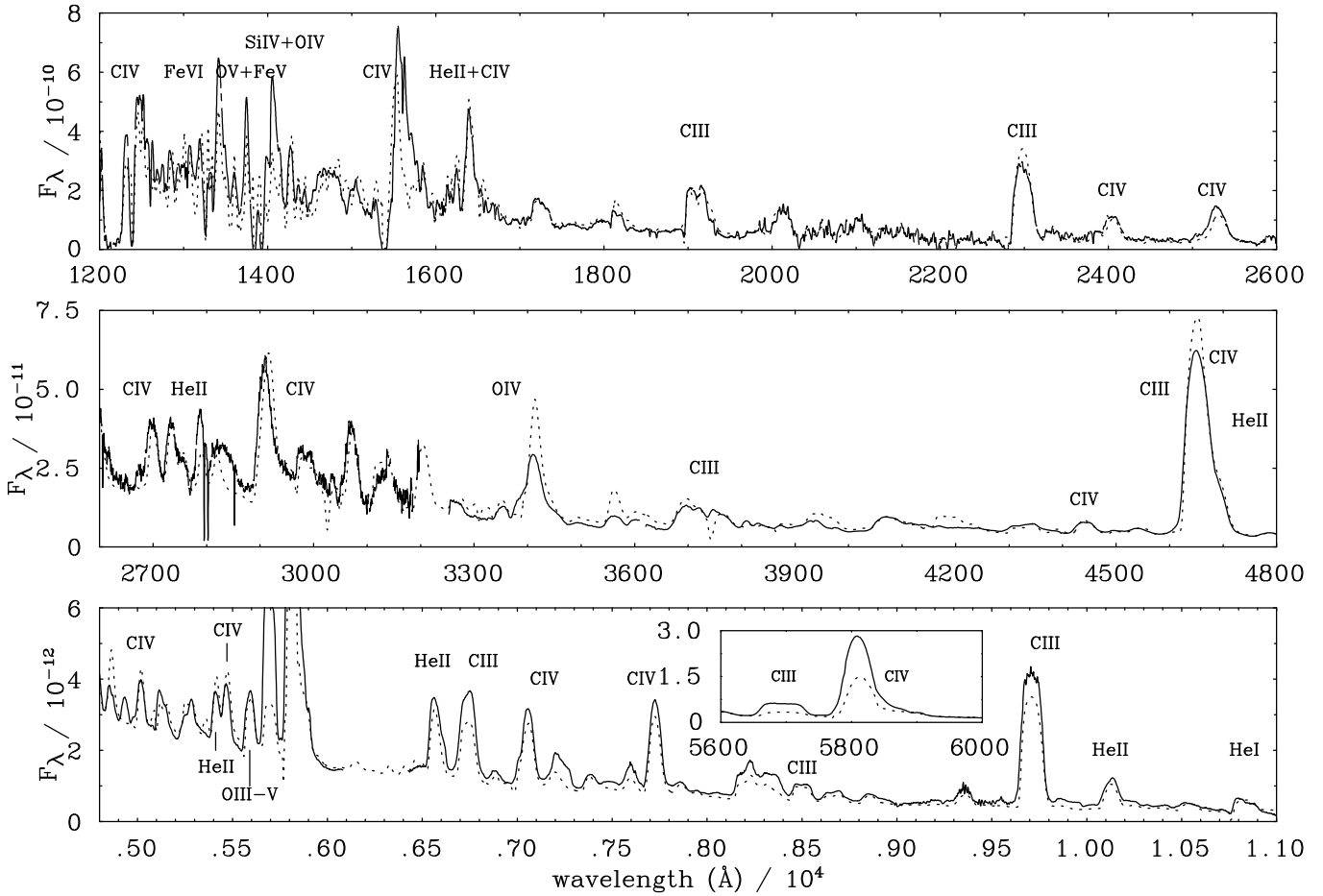


**Figure 10.** Comparison between de-reddened ( $E(B-V)=0.50$  mag) IUE/HIRES and MSSSO/DBS spectroscopy of HD 92809 (solid) with our synthetic model (dotted).

13 features used in the analysis and the relatively small spread in their results. As these are luminous supergiants one must qualify the use of absolute abundance values in any external comparison. For oxygen, magnesium and silicon however the abundances derived in HD167264 (distance from Sun  $\sim 1.7$  kpc; Hill, Walker & Yang 1986) are similar to the absolute values derived in solar-neighbourhood B-type main-sequence stars. The analysis and absolute abundance determination of the dwarfs is more reliable and has been shown to be in excellent agreement with H II regions and the ISM within  $\sim 500$  pc of the Sun (Gies & Lambert 1992, Rolleston et al. 2000). Hence we can be reasonably confident that this agreement means the O, Mg and Si absolute abundances of the HD167264 and OB 10-64 can be used. It appears that the OB 10 cluster was born from an ISM with chemical composition very similar to that of the solar neighbourhood, and given its proximity to the centre of M31 this is a surprising result (see Fig. 12 and Section 5.3).

The similar nitrogen and carbon abundances in the two stars are interesting. MLD in their study of galactic supergiants identified three stellar groupings that they designated as ‘normal’, ‘processed’ and ‘highly processed’ on the basis of their CNO line strengths. By ‘processed’ they meant stars which have C and N line strength ratios which implied that

their photospheres had been contaminated by the products of core CN-cycle burning. HD 167264 was classified as ‘processed’ as it had strong nitrogen lines in comparison with those of carbon. Assuming that the designations of MLD are valid, we conclude that OB 10-64 should also be classified as ‘processed’ and hence at least its carbon and nitrogen abundances may not be representative of its natal composition.

In Section 2.4 we have assumed a distance to M31 of 783 kpc and hence have an estimate of  $M_V = -6.93 \pm 0.4$ . The model atmosphere analysis produces a flux distribution for the stellar parameters shown in Table 4, which provides a bolometric correction of  $-2.9$ . Hence we determine an  $M_{bol} = -9.83 \pm 0.6$ , and  $\log L/L_\odot = 5.85 \pm 0.24$ . This is typical of B-type supergiants (and their possible A-type descendants) as found by Kudritzki et al. (1999), and as illustrated in Fig 8. A comparison with evolutionary models (see Fig 13; Schaller et al. 1992) implies an initial main-sequence mass for the star of approximately  $55M_\odot$ . Whether the star has just come directly from the main-sequence or is a blue-loop star with a previous history as a red supergiant is unclear. The Schaller et al. models predict that the surface CNO abundances should be drastically altered if the star has been a red supergiant and is in a blue-loop. While

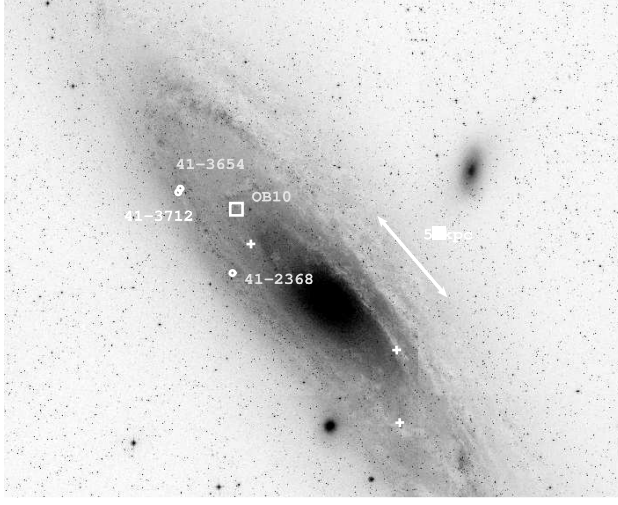


**Figure 11.** A mosaic of DSS images of M31 tiled together (hence the apparent break in the background), with the position of the OB 10 association labelled as the square. For comparison, the positions of three A-F type supergiants analysed by Venn et al. (2000) are shown, with their other star A-207 lying off this field-of-view in the outer south west corner of M31. North is up, east to the left and the size of the image is  $115' \times 90'$ . The three crosses indicate the positions of the three inner disk H II regions analysed by Blair et al. (1982; regions BA75, BA423 and BA289). The length of the double arrow shows 5 kpc at the distance of M31, along the major axis. The projected galactocentric radius of the OB 10 association is 5.9 kpc.

we suggest that it may show some evidence of CNO processing, the quantitative values we derive do not appear to support the star having *highly* processed core material at its surface indicative of a red supergiant origin (where the nitrogen abundance is predicted to be approximately +1.0 dex higher than normal). Whatever its history, its lifetime is likely to have been of the order  $3.5 \pm 1$  Myrs (from Schaller et al. 1992), in excellent agreement with the age of the more evolved WR1 star (with age  $3.6 \pm 0.9$  Myr, see Section 5.2) suggesting coeval formation in the OB 10 association.

## 5.2 Comparison between Galactic, LMC and M31 WC stars

Table 7 reveals that the stellar and chemical properties of OB 10-WR1 and HD 92809 differ substantially, despite originating from very similar environments. Following the mass-luminosity relation for hydrogen-free WR stars of Schaerer & Maeder (1992), a present mass of  $18 \pm 4 M_{\odot}$  is implied. In contrast, the stellar luminosity of HD 92809 is typical of Galactic WCE stars with a present mass of  $\sim 11 M_{\odot}$ . Depending on the choice of evolutionary model, an age within the range 2.7–4.5 Myr is implied for OB 10-WR1.

Since OB 10-WR1 is visually the brightest (apparently single) WCE star in M31 (Massey & Johnson 1998), it is valid to question whether photometry/ spectroscopy of this star is contaminated by bright stars along similar sight lines, particularly since  $1''$  corresponds to a physical scale of  $\sim 4$  pc at the distance of M31. Excess continuum light would serve to dilute the equivalent widths of the WC emission line spec-

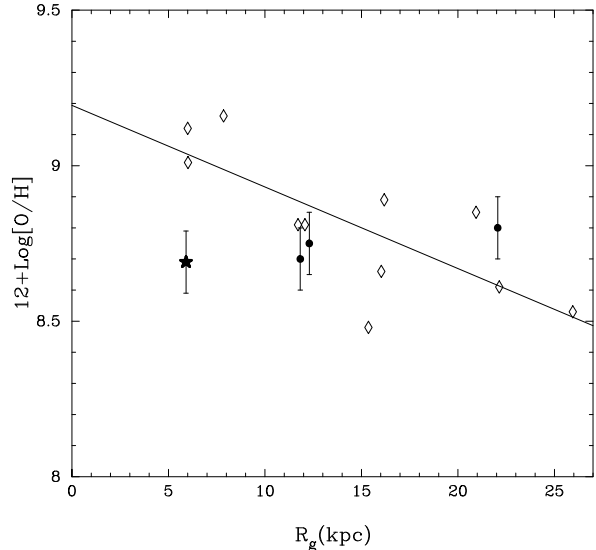


**Figure 12.** Oxygen abundances as a function of distance from the galaxy centre derived in a study of H II regions and the stars so far analysed in M31. The open diamonds are the nebular H II region abundances from Blair et al. (1982), and the line shows the least-squares-fit to these results, giving a gradient of  $-0.03 \pm 0.01$  dex kpc $^{-1}$ . We have recalculated the projected galactocentric distances to the H II regions using an updated distance to M31 of 783 kpc. The solid circles are the oxygen results from Venn et al. (2000), from the three A-F type supergiants shown in Fig. 6. The solid star is our photospheric result from OB 10-64, with the error bar representing the standard error in the mean.

trum, yet from Table 6, the emission line strengths of OB 10-WR1 agree well with the single WC6 star HD 92809. Therefore, in the absence of high spatial resolution imaging we can have confidence that the observed continuum flux is principally that of the WC star, such that its stellar luminosity has not been artificially enhanced.

Galactic WCE stars are known to span a range of carbon abundances and luminosity – according to Koesterke & Hamann (1995)  $0.1 \leq \text{C/He} \leq 0.5$ , and  $5.0 \leq \log L/L_{\odot} \leq 5.4$  for stars with established distances, and applying a global scaling of 0.3 dex to account for blanketing (see Sect. 4.3). Therefore, OB 10-WR1 is amongst the least enriched in carbon, with the highest luminosity. These characteristics are reminiscent of the nearby WC5+OB binary WR146, recently analysed by Dessart et al. (2000) who derived  $\log L/L_{\odot} = 5.7$  and  $\text{C/He} = 0.08$  by number. Extending the comparison to the LMC WCE stars (all WC4 spectral type), reveals quite different conclusions. In contrast with the Galactic sample, the luminosity of OB 10-WR1 is fairly typical of LMC WC4 stars, spanning  $5.4 \leq \log L/L_{\odot} \leq 6.0$ , with comparable C/He abundances established for Brey 10 and Brey 50 (see Fig. 4 in Crowther et al. 2000). Therefore, OB 10-WR1 is more typical of WCE stars at relatively low metallicity. A twice solar metallicity for OB 10 – inferred from H II studies (Blair et al. 1982) – would be very difficult to reconcile with our derived properties of OB 10-WR1.

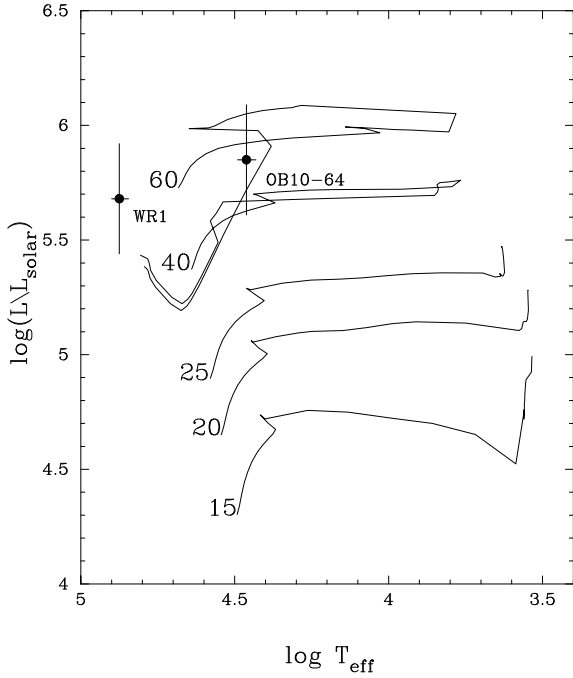


**Figure 13.** The evolutionary tracks from Schaller et al. (1992) are plotted for  $15-60M_{\odot}$  stars, as labeled. The positions of OB 10-64, and WR1 are shown. OB 10 appears to have evolved from  $\sim 36M_{\odot}$  star, whereas WR1 probably evolved from a more massive object. Given the existence of an evolved star of lower mass than WR1, we can infer limits on the time duration of massive star formation in this cluster.

### 5.3 Probing the chemical composition and evolution of M31

In Figure 12 we have plotted the oxygen H II region abundances from Blair et al. (1982) showing the abundance gradient they derive, and the position of OB 10-64. We have recalculated the de-projected galactocentric distances of all the objects in this plot by assuming a distance of 783 kpc, an inclination angle of  $77.5^{\circ}$ , major axis angle of  $37.5^{\circ}$ , and centre of M31 to be RA(2000) =  $00^{\text{h}} 42^{\text{m}} 44^{\text{s}}.4$ , Dec. (2000) =  $41^{\circ} 16' 08''.97$  (the latter from Hjellming & Smarr 1982). The galactocentric distance of OB 10 is 5.9 kpc, and the Blair et al. results suggest that the gas metallicity at this position should be significantly above solar ( $\sim 9.1$  dex). Our absolute abundance of 8.7 dex is well below this value, and while we acknowledge the difficulty in comparing absolute abundances from different methods we are confident that OB 10-64 does not have a metallicity significantly higher than this value – the star has metal-line strengths and atmospheric parameters very similar to those of the Galactic standard HD 167264 as discussed in Section 5.1.

Venn et al. (2000) have presented an analysis of three other stars in M31 (A-F supergiants) and the oxygen abundances for these are also plotted in Figure 12. Fig. 11 also shows the spatial positions of the A-type supergiants and OB10 in the M31 disk. We see that the present results strengthen the suggestion of Venn et al. that the abundance gradient of oxygen is quite flat, extending the stellar results into the supposedly metal rich region interior to

$R_g = 10$  kpc. As noted by Venn et al., neglecting the innermost H II regions results in good agreement between the nebular and stellar results, albeit with a negligible gradient, so it is important to try to understand the current discrepancy in the inner region. In the H II region work the observed quantity used to derive [O/H] is  $R_{23}$ , the ratio  $([\text{OII}]\lambda 3727 + [\text{OIII}]\lambda\lambda 4959, 5007)/\text{H}\beta$ , which is observed to increase with  $R_g$ . This ratio has been calibrated as a function of [O/H] by a number of authors, and indeed as Venn et al. pointed out, using the calibration of Zaritsky et al. (1994) instead of Pagel et al. (1979), reduces the [O/H] abundance gradient from Blair et al.'s value of  $-0.03$  dex kpc $^{-1}$  to  $-0.02$  dex kpc $^{-1}$ . Indeed, within the range of  $R_{23}$  defined by the H II regions in question,  $0.0 \leq R_{23} \leq 0.8$ , there are significant differences between the slopes and absolute values of the various  $R_{23}$  versus [O/H] relationships (see Figure 11 of McGaugh 1991). In fact McGaugh's own calibration results in an even flatter gradient than that of Zaritsky et al. (1994), and systematically lower oxygen abundances by 0.1 to 0.2 dex, with the largest difference being at higher metallicities (see Kobulnicky et al. 1999, equations 9 and 10 for the parameterization). For metallicities above solar there are almost no H II regions for which there are independent estimates of the electron temperature due to the weakness of the [OIII]  $\lambda 4363$  line. Thus the various calibrations in use depend either upon extrapolated empirical relationships, or upon models for which one must make certain assumptions (for example concerning abundances, abundance ratios, model atmosphere fluxes and dust).

Fortunately, Galarza et al. (1999) have presented new results for M31 H II regions between 5 – 15 kpc, and three of these are very close to the OB association OB 10 (regions designated K310, K314 and K315). K315 is spatially coincident with OB 10 and we assume that it is sampling the nebula excited by its OB stars. Interestingly, Galarza et al. (1999) discuss their H II regions by morphological type; center-bright, ring, complex and diffuse, but only those regions defined as center-bright exhibit a significant gradient in  $R_{23}$ . Of the regions mentioned above, only K314 is a center-bright region, it is about 1.5 arc minutes away from OB 10-64, and McGaugh's calibration gives  $12 + \log[\text{O/H}] = 8.98$ , whereas Zaritsky's gives 9.17. We can apply these calibrations to all three H II regions mentioned above, plus the 5 sub-apertures centered on K315 for which Galarza et al. (1999) also give data, which results in oxygen abundances ranging from approximately 8.7 to 9.0 dex using McGaugh's calibration, or from 8.9 to 9.2 dex using Zaritsky's (see Table 8). The former calibration appears to give absolute results in better agreement with the stellar results, indeed our absolute abundance of  $8.69 \pm 0.1$  agrees *within the errors* with the McGaugh calibration of 8.7–9.0 dex. We therefore use this relationship to rederive oxygen abundances using the published H II data from Blair et al. (1982), Dennefeld & Kunth (1981) and Galarza et al. (center-bright regions only). A discussion of which calibration is more physically reliable is outside the scope of this paper, however it seems consistent to homogeneously re-derive the abundances from the full observational dataset using a single relation. We have chosen the McGaugh calibration simply because it provides better agreement with the OB10 stellar results, but would caution against using any one of these calibrations blindly

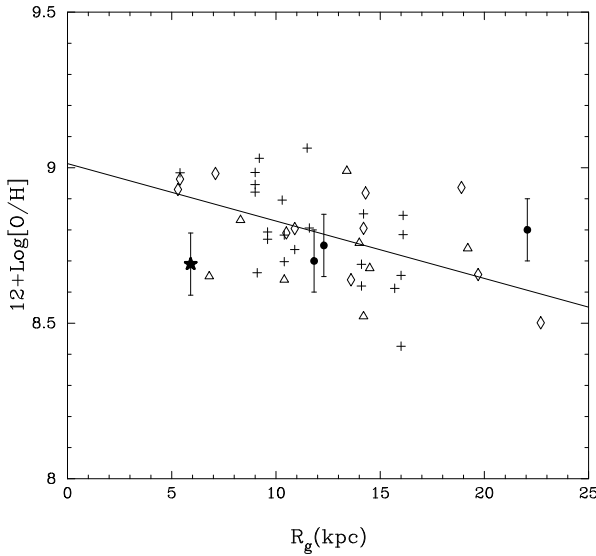


**Figure 14.** All H II region results from Blair et al. (1982; diamonds), Dennefeld & Kunth (1981; triangles) and Galarza et al. (1999; crosses) using the calibration of McGaugh (1991). Stellar points are represented by filled symbols as in Figure 8. The straight line represents a least squares fit to the nebular data giving a gradient of  $-0.018 \pm 0.01$  dex kpc $^{-1}$ .

before more work is carried out on their reliability and the reasons for discrepancies.

These results are shown in Figure 14 together with the stellar results and the least squares fit to the nebular results which gives an oxygen abundance gradient of  $-0.018 \pm 0.01$  dex kpc $^{-1}$ , with an intercept at  $R_g = 0.0$  of 9.02 dex. Note that the corresponding values using Zaritsky's calibration are  $-0.025$  dex kpc $^{-1}$  and 9.22 dex, however the gradient determined from H II regions in the inner, possibly metal rich regions, still depends critically upon the functional form of the calibration used. Clearly this problem can only be resolved by more detailed observations and modelling of these inner regions. The stellar results imply that the [O/H] gradient is extremely flat in the range 5 to 25 kpc. We have not fitted a gradient to the four stars as they are not a homogeneous dataset in terms of their atmospheric parameters and analysis methods; the star analysed here is a B-type supergiant, those at 12 kpc are A-type supergiants, while that at 22 kpc is an F-type supergiant. Certainly, more stellar observations are clearly required, as any gradient which does exist may be masked by statistical scatter or real variations at any particular  $R_g$ .

Without the analysis presented here for OB 10-64 we would have assumed that the initial metallicity of OB 10-WR1 was much higher than solar, and that the wind analysis and stellar evolution discussion would have been based on quite different parameters. This indicates that one must be careful in assuming an initial metallicity determined from global galactic properties when characterising the evolution of single evolved stars, especially WR stars. It is necessary to use more direct methods to determine the state of the natal gas in the environment of the cluster formation.

## 6 CONCLUSIONS

We have carried out detailed, quantitative analyses of high-quality spectral data of two massive stars in the young OB 10 association in M31. This represents the most detailed study of hot, massive stars in this galaxy to date, and shows that quantitative extragalactic stellar astrophysics is not only possible with these objects, but is a powerful diagnostic tool advancing our knowledge in several related areas.

Our analyses allows us to probe massive stellar evolution, mass loss and stellar wind characteristics in the most massive, luminous stars in the Local Universe. We show that we can determine accurate chemical abundances in B-type supergiants which are probes of the current metallicity of the ISM. Our stellar analysis indicates that the empirical calibration of the  $R_{23}$  ratio in H II regions at metallicities of solar and above is not well constrained. Hence when discussing stellar evolution from characteristics of evolved massive stars (WR stars, LBV's, blue and red supergiants) one should be careful to use direct metallicity determinations of the starforming region - photospheric abundance estimates in massive B-type (and A-type, see Venn et al. 2000) supergiants provide an excellent means of doing so.

We have demonstrated that it is possible to analyse the physical and chemical properties of individual WC stars in M31 using 4m class telescopes, although more precise luminosities and abundances await UV spectroscopy. Comparison between OB 10-WR1 and WCE stars in other galaxies, particularly HD 92809 in our Galaxy, reveals that its high luminosity and low C/He ratio is more typical of WCE stars in metal *poor* environments, in spite of the low number statistics. Since OB 10 is in the inner region of the M31 disk ( $R_g = 5.9$  kpc), we would have wrongly concluded that WR1 originated in a very metal *rich* region, had we assumed a metallicity from the previous H II region analysis.

We have carried out a detailed wind-analysis of the B-type supergiant and (assuming previously determined distances to M31) find its wind momentum-luminosity relationship to be in excellent agreement with similar Galactic early B-type stars. This is a further indication (cf Kudritzki et al. 1999), that a properly calibrated wind momentum-luminosity relationship within the Local Group may allow accurate distance moduli to be determined to the most luminous stars in galaxies within  $\sim 20$  Mpc. In further papers we will analyse a larger set of M31 A and B-type supergiants, extending the radial baseline from the central to regions to  $R_g \gtrsim 20$  kpc.

## ACKNOWLEDGMENTS

Spectroscopic data were obtained at the William Herschel Telescope which is operated on the island of La Palma by the Isaac Newton Group in the Spanish Observatorio del Roque de los Muchachos of the Instituto de Astrofísica de Canarias. We are grateful to the staff there for their help in obtaining the observations, and particularly Nic Walton for assistance with some of the Service observing. We acknowledge the usefulness and quick response of the ING Service programme in getting required extra observations. We thank the W.M. Keck foundation and its president Howard B. Keck for the generous grant that made the W.M. Keck Observatory possible. Observations were made through the GO programme

with the NASA/ESA Hubble Space Telescope, and supporting material was obtained from the data archive at the Space Telescope Science Institute. STScI is operated by the Association of Universities for Research in Astronomy, Inc. under NASA contract NAS 5-26555. We gratefully appreciate the use of CMFGEN courtesy of John Hillier. Financial support is acknowledged from the Royal Society (PAC), PPARC (SJS), the Deutsche Zentrum für Luft- und Raumfahrt (DLR) (FB and RPK under grant 50 OR 9909 2), the QUB Visiting Fellowship scheme (SJS and DJL) and the IoA Visiting Fellows scheme (DJL). AH wishes to acknowledge financial support by the spanish DGES under project PB97-1438-C02-01 and from the Gobierno Autonomo de Canarias under project PI1999/008.

## REFERENCES

- Becker S.R., Butler K., 1988, *A&A* 201, 232  
 Becker S.R., Butler K., 1989, *A&A* 209, 244  
 Becker S.R., Butler K., 1990, *A&A* 235, 326  
 Berkhiujsen et al., 1988, *AAS*, 76, 65  
 Bianchi L., Lamers H.J.G.L.M., Hutchings J.B., et al. 1994, *A&A* 292, 213  
 Bianchi L., Clayton G.C., Bohlin R.C., Hutchings J.B., Massey P., 1996, *ApJ* 471, 203  
 Bianchi L., Hutchings J.B., Massey P., 1996, *AJ* 111, 2303  
 Blair W.P., Kirshner R.P., Chevalier R.A., 1982, *ApJ* 254, 50  
 Butler K., 1984, Ph.D. Thesis, University of London  
 Code A.D., Davis J., Bless R.C., Brown R.H., 1976, *ApJ* 203, 417  
 Crowther P.A., Szeifert Th., Stahl O., Zickgraf F.-J., 1997, *A&A* 318, 543  
 Crowther P.A., De Marco O., Barlow M.J., 1998, *MNRAS* 296, 367  
 Crowther P.A., Fullerton A.W., Hillier D.J. et al. 2000, *ApJ* 538, L51  
 Conti P., Massey P., 1989, *ApJ* 447, 251  
 Dennefeld M., Kunth D., 1981, *AJ* 86, 989  
 Dessart L., Crowther P.A., Hillier D.J., Willis A.J., Morris P.M., van der Hucht K.A., 2000, *MNRAS* 315, 407  
 Deutschman W.A., Davis R.J., Schild R.E., 1976, *ApJ Supp.* 30, 97  
 Fitzpatrick E.L., 1986, *AJ* 92, 1068  
 Galarza, V.C., Walterbos, R.A.M., Braun, R., 1999, *AJ* 119, 2775  
 Gies D. R., Lambert D. L., 1993, *ApJ* 387, 673  
 Giddings J.R. 1981, Ph.D. Thesis, University of London  
 Haser S.M., Ph.D. thesis, University of Munich  
 Haser S.M., Lennon D.J., Kudritzki R.P. et al., 1995, *A&A* 295, 136  
 Haser S.M., Pauldrach A.W.A., Lennon D.J. et al., 1998, *A&A* 330, 285  
 Hill G.M., Walker G.A.H., Yang S., 1986, *PASP* 98, 1186  
 Hillier D.J., Miller D.L. 1998, *ApJ* 496, 407  
 Hillier D.J., Miller D.L. 1999, *ApJ* 519, 354  
 Hjellming R.M., Smarr L.L., 1982, *ApJ* 257, L13  
 Holland S., 1998, *AJ* 115, 1916  
 Howarth I.D., Phillips, A.P., 1986, *MNRAS* 222, 809  
 Howarth I.D., Siebert K.W., Hussain G.A., Prinja R.K., 1997, *MNRAS* 284, 265  
 Howarth I.D., Murray J., Mills D., Berry D.S., 1998, *STARLINK User Note SUN 50.21*, Rutherford Appleton Laboratory/CCLRC  
 Hubeny I., 1988, *Computer Physics Comm.* 52, 103  
 Humphreys R.M., Massey P., Freedman W.L., 1990, *AJ* 99, 84  
 Kobulnicky, H.A., Kennicutt, R.C., Pizagno, J.L., 1999, *ApJ* 514, 544  
 Koesterke L., Hamann W.-R., 1995, *A&A*, 299, 503  
 Kilian, J., 1994, *A&A* 282, 867  
 Kudritzki, R.P., 1980, *A&A* 85, 174  
 Kudritzki, R.P., Puls, J., Lennon, D.J., Venn, K.A., Reetz J., Najarro F., McCarthy, J.K., Herrero A., 1999, *A&A* 350, 970  
 Muschielok B., Kudritzki R.P., Appenzeller I., et al. *A&A* 352, L40  
 Lamers H.J.G.L.M., Haser S.M., de Koter A., Leitherer C., 1999, *ApJ* 516, 872  
 Lennon D.J., Dufton P.L., Fitzsimmons A. 1992, *A&AS* 94, 569  
 Lennon D.J., Dufton P.L., Fitzsimmons A. 1993, *A&AS* 97, 559  
 Massey P., Johnson O., 1998, *ApJ* 505, 793  
 Massey P., Armandroff T.E., Conti P.S., 1986, *AJ* 92, 1303  
 Massey P., Armandroff T.E., Pyke R., Patel K., Wilson C.D., 1995, *AJ* 110, 2715  
 McCarthy J.K., Kudritzki R.-P., Lennon D.J., Venn K.A., Puls J., 1997, *ApJ* 482, 757  
 McErlean N.D., Lennon D.J., Dufton P.L., 1999, *A&A* 349, 553  
 McGaugh S.S., 1991, *ApJ* 380, 140  
 Moffat A.F.J., Shara M. M., *ApJ* 320, 266  
 Monteverde M.I., Herrero A., Lennon D.J., Kudritzki R.-P., 1997, *ApJ* 474, L107  
 Monteverde M.I., Herrero A., Lennon D.J., 2000, *ApJ* submitted  
 Pagel, B.E.J., Edmunds, M.G., Blackwell, D.E., Chun, M.S., Smith, G., 1979, *MNRAS* 184, 569  
 Prinja R.K., Barlow M.J., Howarth I.D., 1990, *ApJ* 361, 607  
 Prevot M. L., Lequeux J., Prevot L., Maurice E., Rocca-Volmerange B., 1984, *A&A* 132, 389  
 Rolleston W.R.J., Smartt S.J., Dufton P.L., Ryans R.S.I., 2000, *A&A*, in press  
 Schaerer D., Maeder A., 1992, *A&A* 263, 129  
 Schaller G., Schaerer D., Meynet G., Maeder A., 1992, *A&A Suppl. Ser.* 96, 269  
 Seaton M.J., 1979, *MNRAS* 187, P73  
 Smartt S.J., Dufton P.L., Lennon D.J., 1997, *A&A* 326, 763  
 Smith L.F., Shara, M.M., Moffat, A.F.J., 1990, *ApJ* 358, 229  
 Smith L.J., Crowther P.A., Willis A.J., 1995, *A&A* 302, 830  
 Stanek K.Z., Garnavich P.M., 1998, *ApJ* 503, L131  
 van den Bergh S., 1964, *ApJS* 9, 65  
 Venn K.A., 1995, *ApJ* 449, 839  
 Venn K.A., McCarthy J.K., Lennon D.J., Przybilla N., Kudritzki R.P., Lemke M., 2000, *ApJ*, in press  
 Vrancken M., Lennon D.J., Dufton P.L., Lambert, D.L. 1999, *A&A* submitted  
 Zaritsky, D., Kennicutt, R.C., Huchra, J.P., 1994, *ApJ* 420, 87

This paper has been produced using the Royal Astronomical Society/Blackwell Science L<sup>A</sup>T<sub>E</sub>X style file.

**Table 3.** Equivalent widths,  $W_\lambda$ , for metal lines in OB 10–64 and HD 167264. Typical errors for OB 10–64 are 10% for lines with  $W_\lambda > 70\text{m}\text{\AA}$  and 20% for lines with  $W_\lambda < 70\text{m}\text{\AA}$ . Measurements of  $W_\lambda$  for HD 167264 should normally be accurate to 5%

Wavelength	Species	$W_\lambda$ (m $\text{\AA}$ )		Status
		OB 10–64	HD 167264	
4069.62	O II	400	350	Blended
4069.89	O II			
4070.30	C III			
4071.20	O II	90	100	non-LTE
4072.16	O II			
4075.85	C II	115	145	non-LTE
4075.86	O II			
4253.59	S III	115	110	Blended
4253.74	O II			
4253.98	O II			
4267.02	C II	80	75	non-LTE
4267.27	C II			
4275.52	O II	120	110	non-LTE
4275.90	O II			
4276.21	O II			
4276.71	O II			
4277.40	O II			
4277.90	O II			
4317.14	O II	75	70	non-LTE
4319.63	O II	85	80	non-LTE
4319.93	O II			
4349.43	O II	145	150	non-LTE
4366.89	O II	135	100	non-LTE
4379.05	N III	125	110	LTE
4414.90	O II	110	135	non-LTE
4416.97	O II	135	60	non-LTE
4481.13	Mg II	105	95	non-LTE
4481.33	Mg II			
4510.92	N III	55	90	LTE
4514.89	N III	85	120	LTE
4523.60	N III	40	45	LTE
4590.97	O II	145	90	non-LTE
4595.96	O II	100	70	non-LTE
4596.17	O II			

**Table 3.** continued

Wavelength	Species	Star Number		Status
		OB 10–64	HD 167264	
4609.44	O II	115	70	non-LTE
4610.14	O II			
4630.54	N II	60	55	non-LTE
4631.38	Si IV			
4640.64	N III	230	295	Blended
4641.82	O II			
4641.90	N III			
4647.42	C III	520	405	Blended
4649.14	O II	875	810	Blended
4650.25	C III			
4650.84	O II			
4651.47	C III			
4661.63	O II	75	85	non-LTE
4673.74	O II	170	135	non-LTE
4676.24	O II			

**Table 4.** Stellar atmospheric and wind parameters derived for OB 10–64.

Parameter	Value
$T_{\text{eff}}$	29000 $\pm 1000$ (K)
$\log g$	3.1 $\pm 0.2$ (dex)
$\xi$	10 $\pm 5$ ( $\text{km s}^{-1}$ )
$M$	$1.6 \times 10^{-6}$ $\pm^{0.2}_{0.3} \times 10^{-6}$ ( $M_\odot \text{ yr}^{-1}$ )
$v_\infty$	1650 $\pm 70$ ( $\text{km s}^{-1}$ )
$R_*$	34 $\pm 6$ ( $R_\odot$ )
$\log L/L_\odot$	5.85 $\pm 0.24$ (dex)

**Table 6.** Emission equivalent widths ( $W_\lambda$  in  $\text{\AA}$ ) for selected lines in the optical spectra of OB 10–WR1 and HD 92809, with typical errors of  $\pm 10\%$ . More uncertain values for OB 10–WR1 are shown in parenthesis when strong nebular emission severely contaminates the stellar spectrum

Major	Spectral feature	$W_\lambda$ ( $\text{\AA}$ )	
		Minor	OB 10–WR1 HD 92809
C III $\lambda\lambda 4647-50$	He II $\lambda 4686$	813	881
He II $\lambda 5412$		53	30
C IV $\lambda 5471$		32	40
O V $\lambda\lambda 5572-5604$	O III $\lambda 5590$	35	45
C III $\lambda 5696$		145	198
C IV $\lambda\lambda 5801-12$	He I $\lambda 5876$	1085	907
He II $\lambda 6560$	C IV $\lambda 6560$	(130)	150
C III $\lambda\lambda 6727-60$		(100)	215
C IV $\lambda 7063$	O IV $\lambda\lambda 7032-53$	135	140
C IV $\lambda 7724$	C IV $\lambda 7737$	165	190

**Table 7.** Comparison between stellar parameters of OB 10–WR1 in M31 with the Galactic WC6 star HD 92809 (WR23). Assuming  $M_v$  is appropriate, typical uncertainties are  $\pm 10\text{ kK}$ ,  $\pm 0.12$  dex,  $\pm 100 \text{ km s}^{-1}$ ,  $\pm 0.05$  dex,  $\pm 15\%$  respectively for each parameter.

Star	$T_*$ kK	$\log L$ $L_\odot$	$v_\infty$ $\text{km s}^{-1}$	$\log \dot{M}$ $M_\odot \text{yr}^{-1}$	C/He	$M_v$ mag
OB 10–WR1	75	5.7	3000	−4.3	0.10	−5.4
HD 92809	75	5.3	2280	−4.8	0.30	−4.1

**Table 8.** H II regions observed by Galarza et al. (1999) in the vicinity of OB 10; note that K315 is coincident with the position of OB 10-64 for which we obtain an oxygen abundance of 8.7 dex. Derived abundances  $[\text{O}/\text{H}]_Z$  and  $[\text{O}/\text{H}]_M$  refer to the use of the calibrations of Zaritsky et al. (1994) and McGaugh (1991) respectively.

H II region identifier	Morphological type	$\log(R_{23})$	$[\text{O}/\text{H}]_Z$	$[\text{O}/\text{H}]_M$
K310	diffuse	0.47	9.00	8.85
K314	center-bright	0.24	9.17	8.98
K315	complex	0.39	9.07	8.90
K315a	diffuse	< 0.23	> 9.16	> 8.98
K315b	diffuse	0.23	9.16	8.98
K315c	diffuse	0.16	9.20	9.01
K315d	ring	0.49	9.00	8.83
K315e	ring	0.63	8.84	8.69